Asian Journal of Advanced Research and Reports

Volume 18, Issue 9, Page 151-169, 2024; Article no.AJARR.122194
ISSN: 2582-3248

Strength and Deformation Characteristics of Concrete Beams Reinforced with Glass Fibre Reinforced Polymer Bars

Selase A. K. Kpo [a*], Charles K. Kankam [a], Francis Ohene-Coffie [b], George Oti Boateng [c], Ezekiel Sackitey Nanor [d], John K. Quarm Junior [e] and Edward C. Mansal [a]

[a] Department of Civil Engineering, KNUST, Kumasi, Ghana.
[b] Built Environment Division, CSIR-Building and Road Research Institute, Kumasi, Ghana.
[c] Civil and Environmental Engineering Department, UENR, Sunyani, Ghana.
[d] Department of Civil and Geomatic Engineering, UMaT, Tarkwa, Ghana.
[e] Directorate of Physical Development and Estate Management, UCC, Cape Coast, Ghana.

Authors' contributions

This work was carried out in collaboration among all authors. All authors read and approved the final manuscript.

Article Information

DOI: https://doi.org/10.9734/ajarr/2024/v18i9741

Open Peer Review History:
This journal follows the Advanced Open Peer Review policy. Identity of the Reviewers, Editor(s) and additional Reviewers, peer review comments, different versions of the manuscript, comments of the editors, etc are available here: https://www.sdiarticle5.com/review-history/122194

Original Research Article

Received: 29/06/2024
Accepted: 31/08/2024
Published: 03/09/2024

**Corresponding author: Email: selakay22@gmail.com;*

Cite as: *Kpo, Selase A. K., Charles K. Kankam, Francis Ohene-Coffie, George Oti Boateng, Ezekiel Sackitey Nanor, John K. Quarm Junior, and Edward C. Mansal. 2024. "Strength and Deformation Characteristics of Concrete Beams Reinforced With Glass Fibre Reinforced Polymer Bars". Asian Journal of Advanced Research and Reports 18 (9):151-69. https://doi.org/10.9734/ajarr/2024/v18i9741.*

ABSTRACT

This research presents findings from experiments conducted on the strength and deformation characteristics of concrete beams reinforced with Glass Fiber Reinforced Polymer (GFRP) bars and conventional steel bars as control. The mechanical properties of the GFRP bars and steel bars (10mm and 12mm nominal diameter) used were ascertained. A total of seven (7) reinforced concrete (RC) beams measuring 120mm x 200mm x 2000mm were cast, six (6) of which were GFRP reinforced and one (1) was steel reinforced, and were loaded incrementally until failure. Test variables of two concrete grades, C25 and C30, were adopted in conjunction with two tensile reinforcement ratios of 0.7% and 1.13% for the concrete beams. A uniform compression reinforcement ratio of 0.7% was implemented along with a transverse shear reinforcement ratio of 0.65% for all beams. The data gathered were analyzed using theoretical and experimental approach to provide an insight to deformation characteristics of the reinforced concrete beams cast. An estimation for the theoretical failure load from fracture of tension bars were based on a partial factor of safety (γ_m) of 1.52 for the tensile strength of GFRP. The study examined the deformational behavior including load-deflection response, crack propagation, flexural capacity and failure modes under a four-point monotonic loading test. The experimental results revealed that the GFRP reinforced concrete beams exhibited typical bilinear elastic behavior under static loading with a reduction in stiffness after cracking. The GFRP RC beams failed by sudden concrete crushing due to shear-bond failure, diagonal tension failure in the concrete, and flexural failure in contrast to the steel reinforced concrete beam which failed due to yielding of the steel tension bars. The investigation further highlighted that increasing the concrete compressive strength and the tensile reinforcement ratio of GFRP RC beams significantly improved their structural performance, reducing crack widths and increasing failure loads. GFRP RC beams recorded higher ultimate load capacities and deformations compared to steel-reinforced beams, despite their brittle failure modes. Further aligning with previous research, findings revealed that higher concrete strength leads to a greater number of cracks, but with reduced spacing and narrower widths.

Keywords: GFRP bar; reinforced concrete beams; flexural strength; deformation characteristics; monotonic loading.

1. INTRODUCTION

The construction industry has historically been motivated by the necessity for materials that can improve structural performance while also addressing concerns related to sustainability and durability. Despite its widespread usage, traditional steel reinforcement poses various challenges, such as susceptibility to corrosion, and a substantial carbon footprint linked to its manufacturing process [1]. Glass Fiber Reinforced Polymer (GFRP) bars have emerged as a promising substitute in response to these challenges, offering superior properties like a high strength-to-weight ratio, exceptional corrosion resistance, non-conductivity, electromagnetic resistivity and durability [2-4].

GFRP bars consist of continuous glass fibers incorporated in a polymer matrix, typically epoxy or vinyl ester resin [5]. This composition provides several benefits, including non-corrosive characteristics, which are especially advantageous in settings prone to chemical exposure or moisture, like marine structures, bridges, and wastewater treatment facilities [6]. Moreover, the remarkable tensile strength of GFRP bars renders them an appealing choice for tasks necessitating lightweight yet sturdy reinforcement [4].

Despite the advantages mentioned, the integration of GFRP bars into construction practices has been gradual, mainly due to the limited comprehension of their long-term performance and response under diverse loading conditions. Recent research efforts have concentrated on clarifying the mechanical features of GFRP reinforced concrete structures, leading to notable progress in understanding their tensile strength, bonding behavior, and flexural capacity [7,8]. According to Boateng et al. [7], Issa et al. [9], and Taerwe [10], the GFRP reinforcing bars show a relatively lower modulus of elasticity, reduced ductility, and decreased stiffness when compared to traditional steel. This reduced stiffness, in conjunction with various factors such as altered bond characteristics and decreased tension stiffening, leads to deformations that exceed those of steel-

reinforced elements at all loading stages. As a result of these significant deformations, the design of structures might be influenced by constraints related to deflection [11]. Nonetheless, extensive investigations on the strength and deformation properties of GFRP reinforced concrete beams remain relatively scarce.

The strength of a reinforced concrete beam is a vital parameter that determines its capacity to sustain loads without any structural failure [12]. In the instance of GFRP reinforced concrete beams, this covers not just the ultimate load-carrying capability but also the beam's response under various load forms. Contrarily, deformation characteristics offer valuable insights into how a beam reacts to applied loads concerning deflections and crack development [13,14]. The comprehension of these characteristics is essential in evaluating the serviceability and durability of GFRP-reinforced beams. Unlike steel, GFRP bars display a linear elastic response until failure without yielding, influencing the ductility and energy absorption potential of the reinforced concrete structures [7,15,16].

Experimental and numerical investigations have revealed that the incorporation of GFRP bars led to improvements in the flexural strength of concrete beams, where different reinforcement ratios had varying impacts on load-bearing capacity and deflection [17]. Results from the studies showed promising outcomes for the use of GFRP bars in concrete structures, demonstrating higher failure loads and deflections compared to traditional steel reinforcement, particularly in cases involving lower strength concrete beams [18]. The findings also highlighted the variation in behavior of GFRP-reinforced concrete beams based on tensional reinforcement ratios, indicating that the role of GFRP bars in the compression zone was negligible in design considerations. Adam et al. [19] concluded that increasing the concrete strength and the reinforcement ratio of GFRP reinforced concrete beams can lead to a substantial improvement in their flexural performances as they can reduce the crack widths. Zhang et al. [20] researched on the bonding performance between GFRP bars and reported that concrete is significantly affected by the deformation characteristics of the bars, where higher deformation coefficients can enhance bond strength but may result in a transition of failure modes from ductile to brittle. Xie et al. [21] also had similar findings.

Muhamad [22] made an experimental inquiry involving full-scale assessments of GFRP-reinforced beams under controlled settings and provided significant insights into their response to load-induced deformations, failure mechanisms, and patterns of crack propagation. One of the crucial parameters for evaluating the structural behavior of reinforced concrete beams is the measurement of crack width and its progression. Numerous studies [23-25] have indicated that both crack width and propagation have the potential to diminish the stiffness of the beam, resulting in augmented deflections and decreased structural efficiency. The existence of wide cracks may lead to a reduction in the load-carrying capacity of the beam, thereby increasing the chance of premature structural failure. Besides, the occurrence of cracks can expose the embedded reinforcement to moisture, leading to the initiation of corrosion processes that jeopardize the structural integrity. In beams with low ductility, wide cracks can escalate the susceptibility to brittle failure. Additionally, the presence of cracks enables the penetration of water and aggressive substances, giving rise to durability concerns and possible deterioration of the structural elements [1].

This experimental study sought to enhance the understanding of the strength and deformational characteristics of GFRP-reinforced beams under static loading conditions, thereby facilitating their effective application in structural engineering.

2. EXPERIMENTAL PROGRAM

2.1 Materials

The components that were integrated included fine aggregate, coarse aggregate, ordinary Portland cement, GFRP reinforcing bars, reinforcing steel bars as control and potable water. Fine aggregate comprised natural pit sand with a maximum particle size of 4.75 mm, while coarse aggregate consisted of crushed granite with a maximum size of 12.5 mm. Both fine and coarse aggregates underwent a sieve analysis that adhered to BS 1377: 1990 [26] standards, and the cement, met the specifications of ASTM C150 [27]. The GFRP bars were ribbed and sand coated, with diameters of 10mm and 12mm. All the materials used in this experimental study including the GFRP bars were locally produced in Ghana, indicating the feasibility of implementing GFRP technology in the construction industry within the country.

2.2 Preparation of Test Specimens

2.2.1 Mix design

Two concrete mix ratios were employed comprising 1:2:3, 0.45 and 1:1:2, 0.4 (cement: fine aggregate: coarse aggregate, w/c) for the intended concrete strength of C25 and C30 respectively in accordance with IS:10262 (1982) [28].

2.2.2 Mixing, casting and curing

Initially, the fine aggregate and cement were proportioned and poured into a mechanical concrete mixer, followed by the addition of coarse aggregate. These materials were mixed in a dry state for around two minutes, after which water was gradually introduced to the dry mixture. The mixing process was standardized, resulting in a consistent appearance in a plastic mix. To ensure thorough blending, the blending time was approximately 2 minutes per rotation. A slump test was performed to assess the workability of the concrete.

2.3 Preparation of GFRP Bars

The longitudinal tensile reinforcement ratios and transverse reinforcement ratio (stirrups) were parameters examined for the GFRP bars. Two longitudinal tensile reinforcement ratios of 0.7% (2ø12 mm GFRP bars) and 1.13% (3ø12 mm GFRP bars) together with a transverse shear reinforcement ratio of 0.65% (ø10mm, 200mm stirrup spacing) were adopted. The GFRP reinforcement ratios described above resulted in two configurations which are detailed in Fig. 1, in addition to the reinforcement cages fabricated.

2.4 Preparation of Reinforced Concrete Beams

Marine board was employed as the material for the concrete beams and control specimen formwork, configured to specified dimensions of 120 mm in width, 200mm in depth, and 2000mm in length for the beam. Lubrication was applied to the inner surface of the beam formwork using recycled engine oil to facilitate easy removal post-casting. After being filled with concrete and compacted, attention was given to achieving a consistent cover below and around the reinforcement, and the surface of the cast concrete was smoothened. A total of seven (7) beams were cast. Two concrete grades of C25 and C30 were adopted together with two tensile reinforcement ratios of 0.7% and 1.13%. Compression reinforcement comprising two bars of 12mm diameter that was equivalent to 0.7% of beam cross-section was also adopted. Furthermore, stirrups reinforcement comprising 10mm diameter bars at 200mm spacing (equivalent to 0.65% ratio) was used for all the beams. The reinforcement types and configurations, beam cross-sectional dimensions, along with cube strength and modulus of rupture for all the beams are presented in Table 1. Additionally, concrete cubes (150x150x150mm) and prisms (100x100x500mm) were cast as control for compressive strength and modulus of rupture respectively. After 24 hours, the beams and control specimens were extracted from their molds and subjected to a curing process under wet hessian cloth for 28 days. Prior to testing, they were thoroughly cleaned of any debris and coated with white emulsion paint on all surfaces.

2.5 Test Procedures

2.5.1 Concrete compressive strength test

Compressive strength of the cured concrete cubes for both concrete mixes (1:2:3, 0.45 and 1:1:2, 0.4) was determined at 7 days, 14 days and 28 days in accordance with BS EN 12390-3 [29], using the Universal Testing Machine (UTM). Cube designed for C25 strength exhibited average compressive strengths of 16.3 N/mm^2, 20.9 N/mm^2, and 23.4 N/mm^2 at the age of 7 days, 14 days, and 28 days, respectively. Furthermore, cube designated for C30 strength demonstrated average compressive strengths of 20.1 N/mm^2, 27.1 N/mm^2, and 30.4 N/mm^2 after 7 days, 14 days, and 28 days respectively as shown in Table 2.

2.5.2 Concrete modulus of rupture test

The concrete prism (100mm x 100mm x 500mm) was simply supported over a span of 400mm in a rigid steel framework and loaded with a central point load until failure. The modulus of rupture for the designated C25 concrete prism was 5.4 N/mm^2, whilst that for the designated C30 concrete prism was 6.3 N/mm^2 (Table 3).

2.5.3 Tensile test

The tensile strength of the GFRP reinforcing bars was obtained by employing the Universal Testing Machine (UTM) based on the protocols specified in ASTM D7205 [30]. Specimens of 10mm and 12 mm diameters were initially prepared by

securing grip at each end with a 25mm steel pipe having an inner diameter of 22mm. The GFRP bars were inserted 150mm into the steel pipe grips at both ends, thus resulting in a 300mm free length. An epoxy mixture (Bisphenol A) enriched with expanding additives and distinguished by high-strength non-shrink properties was employed to fill the void between the steel pipe and GFRP bar. The specimens underwent a sealing process and were permitted to cure for a duration of 24 hours, followed by a subsequent three-day period for hardening.

The tensile test was carried out in a 1000 kN capacity ELE universal testing machine featuring an extensometer of 50mm gauge length. Tension was applied to the bar at a constant rate of 3mm per minute until failure. Various failure modes, including fiber glass fracture or epoxy failure were recorded, along with tensile strength, Young's modulus of elasticity, failure strain, and automatic plotting of stress-strain curve. Additionally, tensile test was conducted on the reinforcing steel bars. The results of tensile test are presented in Tables 4 and 5.

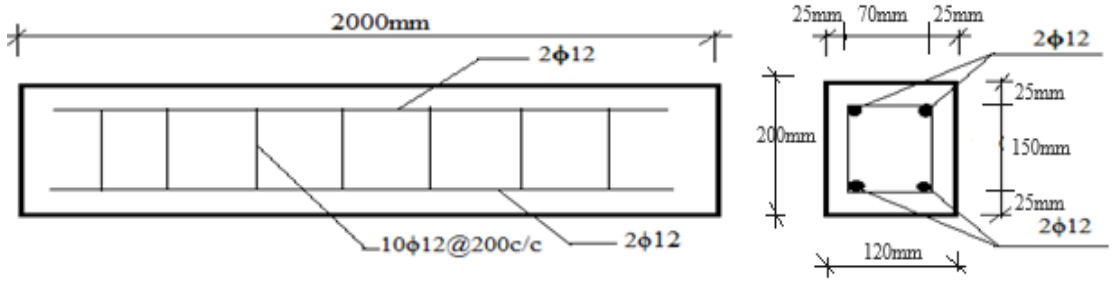

(a) Beam configuration A

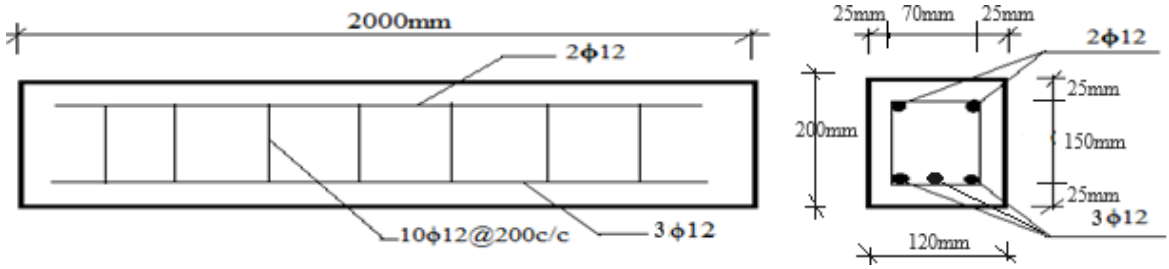

(b) Beam configuration B

(c) Fabricated GFRP cages

Fig. 1. Preparation of reinforcement

Table 1. Details of beam specimens

Beam ID	Reinforcement type	Cross section b x d (mm^2)	Cube strength (N/mm^2)	Modulus of rupture (N/mm^2)	Compression reinforcement ratio, ρ (%)	Tensile reinforcement ratio, ρ (%)	Stirrups (%)
BG1	GFRP	120x200	23.4	5.4	0.7	0.7	0.65
BG2	GFRP	120x200	30.4	6.3	0.7	0.7	0.65
BG3	GFRP	120x200	30.4	6.3	0.7	0.7	0.65
BG4	GFRP	120x200	23.4	5.4	0.7	1.13	0.65
BG5	GFRP	120x200	23.4	5.4	0.7	1.13	0.65
BG6	GFRP	120x200	23.4	5.4	0.7	1.13	0.65
BS1	Steel	120x200	23.4	5.4	0.7	0.7	0.65

Table 2. Compressive strength of cube specimens

Specimen Target Strength	Average Compressive Strength (N/mm²)		
	7 days	14 days	28 days
C25	16.3	20.9	23.4
C30	20.1	27.1	30.4

Table 3. Modulus of rupture of concrete prism specimens

Specimen Target strength	Average Maximum Load (N)	Average Modulus of Rupture (N/mm²)
C25	9044.3	5.4
C30	10463	6.3

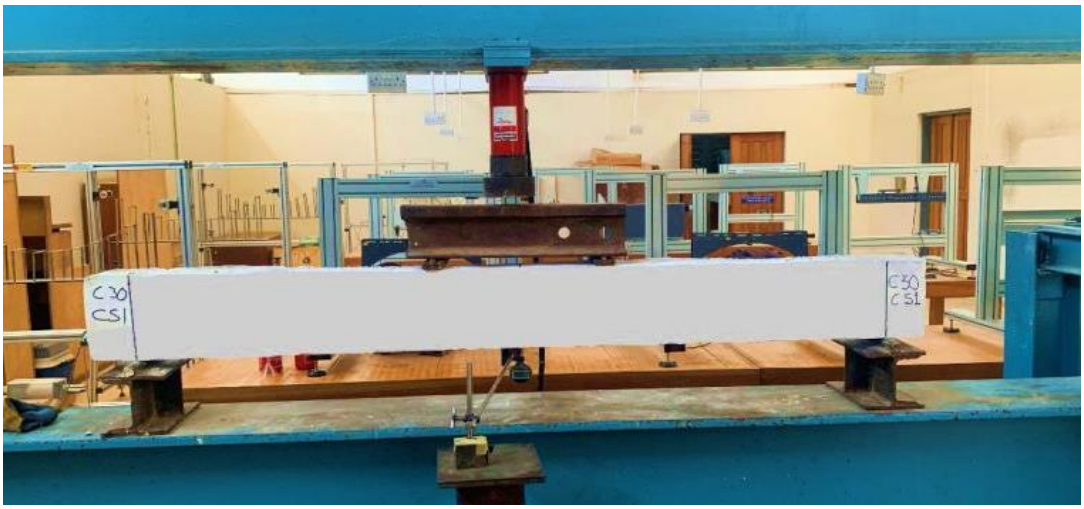

Fig. 2. Beam testing set-up

2.5.4 Testing of reinforced concrete beams

The cured beams at maturity of 28 days were cleaned and painted white in order to clarify the crack detection. The beams were placed in a rigid steel loading frame equipped with two supports positioned 100 mm from the beam ends, with a clear span of 1,800 mm. An actuator comprising a hydraulic jack and an attached load cell was employed to apply the load at 2kN intervals through a rigid spreader steel beam that was used to transfer the load to the specimen through two symmetrical loading points 400 mm apart, with both load points having a distance of 700mm to the nearest support as illustrated in Figs. 2 and 4. The deflection and crack patterns were monitored, measured and recorded. At the failure loads, corresponding to the point of beam failure, the crack propagation parameters such as crack width, spacing and types of cracks were recorded for analysis. The recorded data were used to establish the load-deflection relationship and provide insights into beam behavior under the varying loads.

3. RESULTS AND DISCUSSION

3.1 Mechanical Properties of Reinforcement Bar Specimens

The mechanical properties for the traditional mild steel bars and GFRP bars are presented in Tables 4 and 5 respectively. The 10mm and 12mm diameter GFRP bars exhibited ultimate tensile strengths of 1193 N/mm² and 1030 N/mm² respectively. The Young's modulus of elasticity of the GFRP bars were determined as 54.43 kN/mm² and 41.71 kN/mm² for the 10mm and 12mm bar sizes, respectively. Furthermore, the ultimate elongation values are recorded at 2.20% and 2.48% for the 10mm and 12mm GFRP bars, respectively.

As illustrated by Fig. 3, the stress-strain relationship observed for the GFRP bars is characterized by a linear trajectory; as the applied stress increases, the resultant strain increases proportionally until the ultimate strength is attained, where failure occurs. The

stress–strain curves of GFRP bars demonstrate a notable absence of a distinct yield point, as associated with the response of steel bars that depicts a typical combination of linear and non-linear behaviors in their stress–strain characteristics and are commonly indicative of ductile failure modes in structural frameworks, where considerable prior warning of potential failure is observed. Notwithstanding its lack of a well-defined yielding stage characteristic, the high strain capacity combined with a low modulus of elasticity throughout the entire elastic range makes GFRP bar suitable for resisting large stresses [7,10].

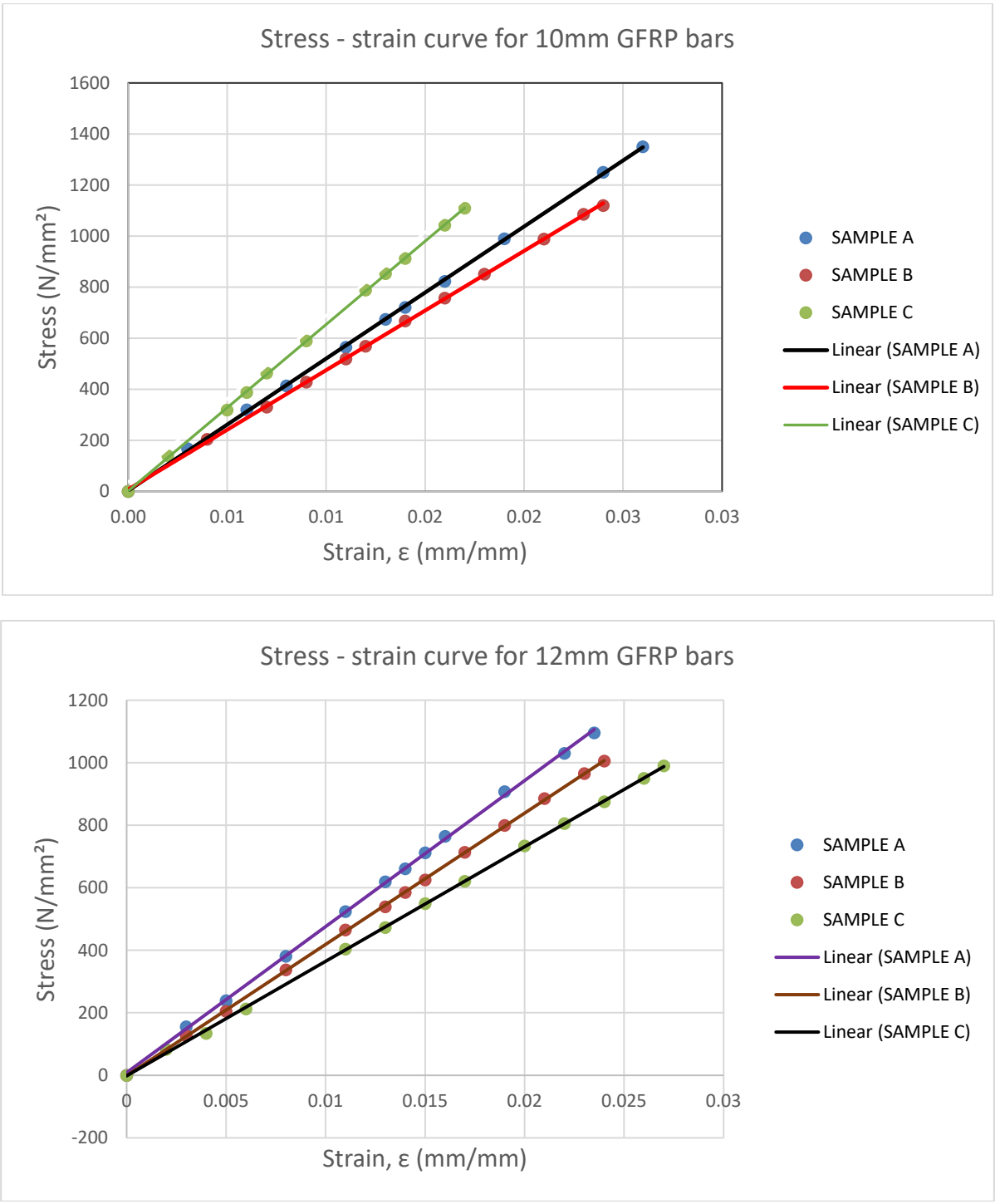

Fig. 3. Stress-strain curve for 10 mm and 12 mm GFRP bars

Table 4. Mechanical properties of traditional steel reinforcing bars

Bar Diameter	Average Diameter (mm)	Yield Strength (N/mm^2)	Yield Strain (E_v)	Tensile Strength (N/mm^2)	Average Ultimate Elongation (%)
10 mm	9.24	464.20	0.0026	545.19	18.03
12 mm	11.17	457.57	0.0031	538.30	18.7

Table 5. Mechanical properties of GFRP bars

Bar Diameter	Average Diameter (mm)	Average Ultimate Tensile Strength (N/mm^2)	Average Young's Modulus of Elasticity (kN/mm^2)	Average Ultimate Elongation (%)
10 mm	9.54	1193	54.43	2.20
12 mm	11.35	1030	41.71	2.48

Table 6. Deflections and crack modes

Beam ID	Deflection at first crack, (mm)	Final deflection (mm)	Maximum crack width (mm)	Average crack spacing (mm)	Types and No. of cracks		
					No. of pure shear cracks	No. of pure flexural cracks	No. of flexural shear cracks
BG1	0.98	28.86	1	97.5	4	5	4
BG2	9.04	19.53	1	55.54	6	6	3
BG3	2.52	20.3	1	50.52	6	8	3
BG4	5.19	19.88	0.5	71.88	5	6	3
BG5	7.99	18.54	1	68.9	4	4	7
BG6	4.66	20.38	0.5	91.57	3	6	5
BS1	4.43	11.39	2	54.83	6	7	9

3.2 Theoretical Flexural Analysis

The theoretical analysis was caried out to establish the theoretical cracking loads from the cracking moment equation (Eqn. 1-2). Furthermore, theoretical failure loads were based on assumptions of either the GFRP bar failing first or concrete crushing occurring first or shear failure occurring first (Eqn. 3-6). Consequently, the results of the computations from the theoretical analysis as well as the experimental data are captured in Table 7.

3.2.1 Cracking moment

3.2.1.1 Cracking moment of reinforced concrete beam (M_{cr})

For a reinforced concrete beam, the cracking moment (M_{cr}) is obtained employing the modulus of rupture (f_t) in the expression as in Eqn. 1, assuming elastic behavior;

$$M_{cr} = f_t \frac{bd^2}{6} \quad \ldots\ldots\ldots\ldots\ldots\ldots\ldots\ldots\ldots (1)$$

where M_{cr} is the cracking moment (Nmm); f_t is the modulus of rupture (N/mm^2); b = width of beam (mm); d = depth of beam (mm).

3.2.2 Theoretical cracking load of RC beam

From the 4-point loading system of the RC beam in Fig. 4., the theoretical cracking load of the beam can be expressed as shown in Eqn. 2;

$$P = \frac{2M}{L_1} \quad \ldots\ldots\ldots\ldots\ldots\ldots\ldots\ldots\ldots\ldots (2)$$

where P = P_{cr}; P_{cr} is the theoretical cracking load (kN); M = M_{cr} is the cracking moment (kNm); L_1 is distance from the support to the nearest load point (700mm). Computed values of theoretical cracking loads for the RC beams are shown in Table 7.

3.2.3 Analyses of theoretical failure load

The analysis of the theoretical failure load is based on three main assumptions, namely; (i) GFRP bar failing first, (ii) concrete crushing first or (iii) shear failure occurring first.

3.2.4 Theoretical failure load based on GFRP bar failing first

For the simply supported shown in Fig. 4, the ultimate load is expressed by Eqn. 3 as follows;

$$P_{ult} = \frac{2M_{rf}}{L_1} \quad \ldots\ldots\ldots\ldots\ldots\ldots\ldots\ldots\ldots\ldots (3)$$

where M_{rf} is the moment of resistance of GFRP bar in tension (kNm); P_{ult} is the ultimate failure load for GFRP bar (kN); L_1 is distance from the support to the nearest load point (700 mm).

With partial factor of safety of 1.52 [7], the moment of resistance of the GFRP in tension is given by;

$$M_{rf} = 0.66 f_{yf} A_f * 0.775\mathrm{d} \ldots\ldots\ldots\ldots\ldots\ldots\ldots (4)$$

where f_y is the tensile strength of GFRP bar (N/mm^2); A_f is area of GFRP in tension zone (mm^2); d is the effective depth of beam (mm).

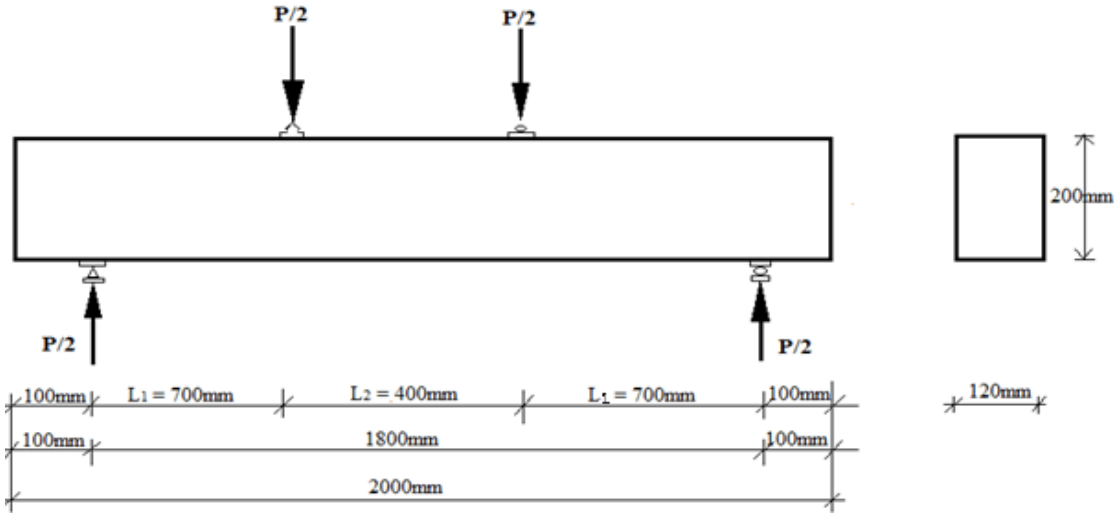

Fig. 4. Schematic diagram of 4-point loading system for beams

Table 7. Cracking and failure loads of beams

Beam ID	Theoretical cracking load, P_{cr} (kN)	Experimental cracking load, P'_{cr} (kN)	Theoretical Failure load P_{ult} (kN) based on			Experimental failure load, P'_{ult} (kN)	P'_{cr}/P_{cr}	P'_{ult}/P_{ult}
			Reinforcement failing	Concrete Crushing	Shear Failure			
BG1	12.3	12	52.3	37.0*	98.6	28	0.96	0.76
BG2	14.4	16	52.3	48.1*	98.6	28	1.11	0.58
BG3	14.4	16	52.3	48.1*	98.6	36	1.11	0.75
BG4	12.3	14	78.6	37.0*	98.6	30	1.14	0.81
BG5	12.3	16	78.6	37.0*	98.6	30	1.3	0.81
BG6	12.3	16	78.6	37.0*	98.6	28	1.3	0.76
BS1	12.3	20	30.6	70.5	63.4	30	1.6	0.98
Average:							1.15	0.75

*Note: *Governing failure load of beam*

Three (3) categories of tensile reinforcement were employed in the beam specimen; namely; ratios of 0.7% and 1.13% GFRP bars and 0.7% steel tensile reinforcement in control beams are shown in Table 7.

3.2.5 Theoretical failure load based on concrete crushing first

Theoretical failure load of a reinforced concrete beam based on concrete crushing first in compression is given as expressed by Eqn. 6 including compression bar;

$$P_{ult} = \frac{2M_{rc}}{L} \quad \ldots\ldots\ldots\ldots\ldots\ldots\ldots\ldots (5)$$

$$M_{rc} = 0.156 f_{cu} bd^2 + \gamma_m f_{fy} A_f (d - d^1) \quad \ldots\ldots\ldots\ldots\ldots (6)$$

where M_{rc} is the Moment of resistance of concrete beam (kNm); P_{ult} is the Concrete crushing load (kN); f_{cu} is the concrete compressive strength (N/mm^2); γ_m is the partial factor of safety; d^1 is the effective depth of compression GFRP bar; A_f is the area of GFRP bars in compression (mm^2). The computed values of failure loads of the RC beams assuming concrete crushes first are captured in Table 7 without contribution by GFRP bars in compression [18].

3.2.6 Theoretical failure load based on the assumption of shear failure occuring first

$$V_f = 0.66 \frac{A_{sv}}{S_v} f_y * d + V_c bd \ldots\ldots\ldots\ldots\ldots\ldots (6)$$

where V_f is the shear failure load (kN); f_y is the yield strength of GFRP stirrups (N/mm^2); V_c is the design concrete shear strength (kN); A_{sv} is the area of shear reinforcement (mm^2); S_v is the spacing of stirrups; b is the width of the beam (mm).

Results of the computations for shear failure occurring first for beam specimens are captured in Table 7.

4. THEORETICAL AND EXPERIMENTAL RESULTS

4.1 Cracking Moment

The cracking loads of the tested beams are detailed in Table 7. Specifically, the experimental cracking load values for the GFRP RC beams ranged from 12k N to 16 kN, while the steel reinforced beam had an experimental cracking load at 20 kN. The experimental cracking loads (P'_{cr}) of the beams reinforced with GFRP bars averaged 1.15 (15% higher) of the theoretical cracking loads (P_{cr}). However, the beams reinforced with steel reinforcing bars achieved experimental cracking loads (P'_{cr}) 1.6 (60% higher) of the theoretical cracking loads (P_{cr}). It is noteworthy that the cracking load is closely associated with the tensile strength of concrete, a property dependent on compressive strength. As such, an increase in concrete compressive strength resulted in higher cracking moments.

4.2 Load-Deflection Behavior

Fig. 5 illustrates typical bilinear load-deflection relationships for seven reinforced concrete beams. Six beams were reinforced with GFRP bars, while one beam was reinforced with traditional mild steel bars. In general, the load-deflection curves of the GFRP RC beams can be categorized into two distinct phases; the initial phase is commonly known as the "pre-crack stage," during which the behavior exhibited by all beam specimens demonstrated a steep and nearly linear trend. Subsequently, the succeeding phase is referred to as the "post-cracking stage," characterized by the initiation and progression of cracks within the specimens. During this latter phase, the further crack propagation into the concrete compression zone led to a reduction in the flexural stiffness of the beams, until failure due mainly to concrete crushing.

4.3 Crack Propagation and Crack Width

Details of the types of cracks, their propagation and crack widths are presented in Table 6. The average crack spacing values ranged from 50.52 mm to 97.5mm for the GFRP reinforced beam while the steel reinforced beam recorded an average spacing of 54.83mm. Moreover, crack width values ranged from 0.5 mm to 1 mm for the GFRP reinforced beams whereas the steel reinforced beam recorded a 2 mm crack width. The types and number of cracks developed are also shown in Table 6. A noticeable trend is that increasing reinforcing ratio in GFRP-RC beams led to an increase in the quantity of cracks and consequently a reduction in the average crack spacing. Furthermore, Table 6 highlights the influence of concrete compressive strength on crack propagation. When subjected to equivalent load conditions, an increase in concrete strength

resulted in a higher number of cracks characterized by decreased inter-crack spacing and diminished crack widths in contrast to beams composed of concrete with lower strength, as confirmed by previous research [12,21].

4.4 Failure Loads

Table 7 presents the theoretical and experimental failure loads of the beams under monotonic loading conditions. The average experimental failure load (P'_{ult}) of the GFRP RC beams were approximately 75% of the theoretical failure load (P_{ult}). On the other hand, the experimental failure load (P'_{ult}) observed for the steel reinforced concrete beams was found to be 98% of the theoretical ultimate failure loads.

It can be observed from Table 7 that the experimental failure loads (P'_{ult}) of the GFRP RC beams ranged between 28 kN and 36 kN. Beam BG3, with a compressive strength of 30.4 N/mm^2, exhibited a higher experimental failure load compared to beam BG1, with compressive strength of 23.4 N/mm^2. This indicates that an increase in the concrete compressive strength of GFRP RC beams caused an increase in the failure load. Adam et al. [1] and Yang [5] also had similar findings. As depicted in Table 7, GFRP RC beam BG1, with a longitudinal tensile reinforcement ratio of 0.7%, experienced a lower ultimate load of 28 kN in contrast to beam BG4, with a longitudinal tensile reinforcement ratio of 1.13%, which failed at 30 kN. This pattern demonstrates that a greater longitudinal reinforced GFRP RC beam results in a higher failure load, and vice versa.

4.5 Flexural Capacity and Mode of Failure

The simply supported beam in this study that is subjected to monotonic loading has a maximum constant bending moment and zero shear across the central span. The remaining two spans, on the other hand, experience maximum shear forces and varying bending moment magnitudes under different loads. The central span of each beam specimen was found to be the location of the first crack, indicating the location of the greatest strain. The GFRP reinforced concrete beams failed by concrete crushing. This was due to shear-bond failure, diagonal tension failure in the concrete, and flexural failure brought on by concrete crushing as reported by Xie et al. [21] and Kim [24]. On the other hand, the steel-RC beam failed due to yielding of the steel tension bars. Figs 6 to 12 show the various beams at failure.

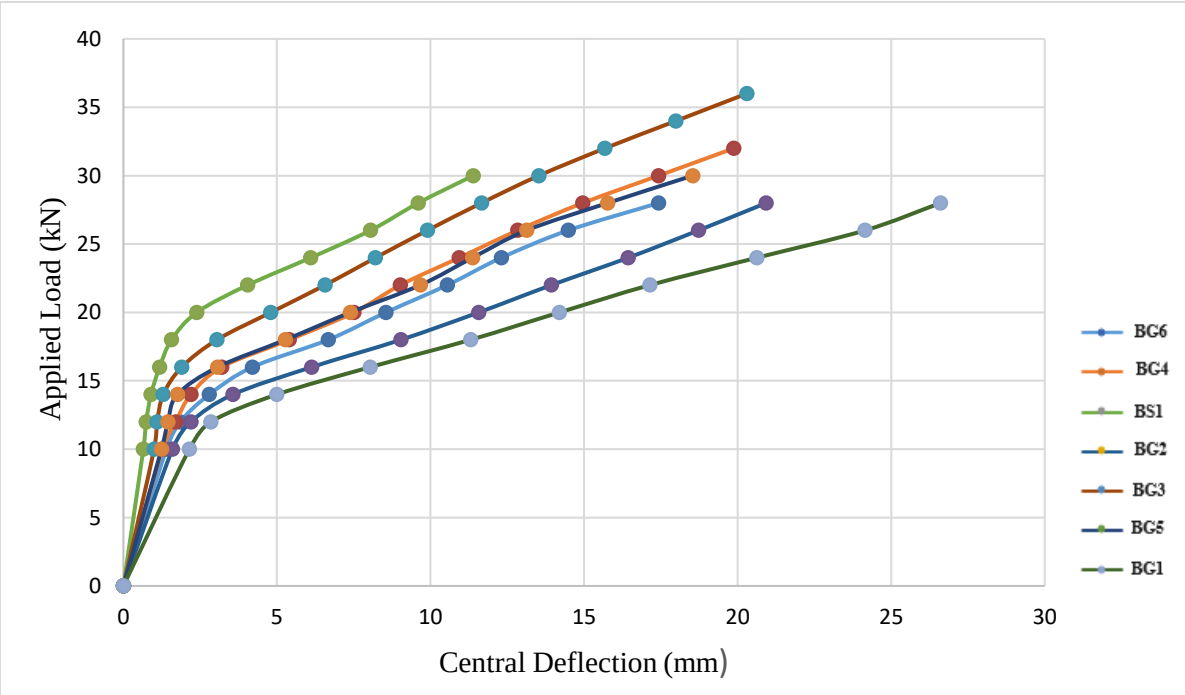

Fig. 5. Load - deflection response

Fig. 6. Beam BG1 failure mode

For beam BG1 shown in Fig. 6, the beam had longitudinal tensile reinforcement ratio of 0.7%, a transverse reinforcement ratio of 0.65%, a 23.4 N/mm^2 cube strength and a 5.4 N/mm^2 modulus of rupture. The beam failed with 4 pure shear cracks, 5 flexural cracks within the constant moment span and 4 flexural cracks at the shear span area of the beam. A maximum crack width of 1mm was measured with an average crack spacing of 97.5mm. The first crack appeared at 12 kN loading with a corresponding deflection of 0.98 mm. At 28 kN loading, the beam underwent a sudden brittle failure at a final deflection of 28.86 mm.

The beam BG2 in Fig. 7 had longitudinal tensile reinforcement ratio of 0.7%, a transverse reinforcement ratio of 0.65%, a 30.4 N/mm^2 cube strength and a 6.3 N/mm^2 modulus of rupture. The beam failed with 6 pure shear cracks, 6 flexural cracks within the loaded span and 3 flexural cracks at the shear span area of the beam. A maximum crack width of 1mm was measured with an average crack spacing of 55.45mm. The first crack appeared at 16 kN loading with a corresponding deflection of 9.04 mm. At 28 kN loading, the beam underwent a sudden brittle failure at a final deflection of 19.53 mm.

For beam BG3 in Fig. 8, it had a longitudinal tensile reinforcement ratio of 0.7%, a transverse reinforcement ratio of 0.65%, a 30.4 N/mm^2 cube strength and a 6.3 N/mm^2 modulus of rupture. The beam failed with 6 pure shear cracks, 8 flexural cracks within the loaded span and 3 flexural cracks at the shear span area of the beam. A maximum crack width of 1mm was measured with an average crack spacing of 50.52mm. The first crack occurred at 16 kN loading with a corresponding deflection of 2.52 mm. At 38 kN loading, the beam underwent a sudden brittle failure at a final deflection of 20.3 mm.

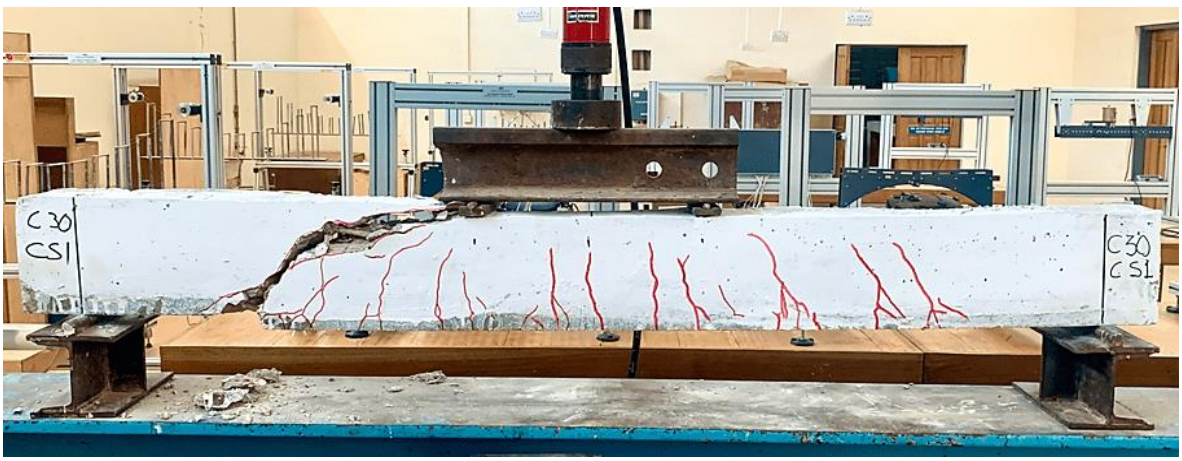

Fig. 7. Beam BG2 failure mode

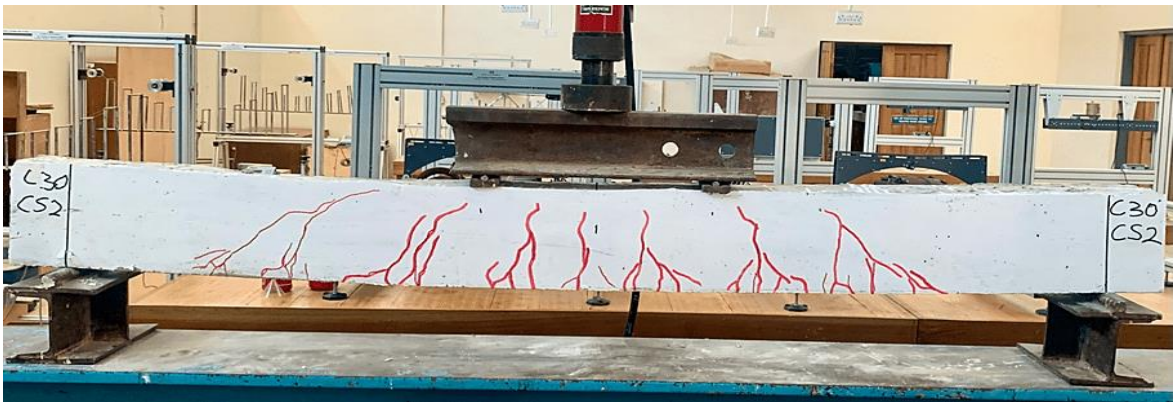

Fig. 8. Beam BG3 failure mode

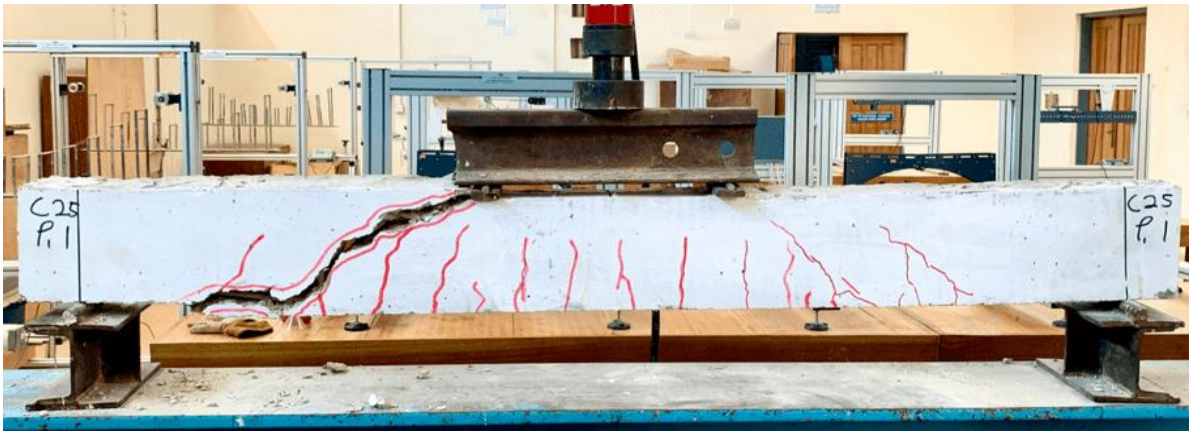

Fig. 9. Beam BG4 failure mode

The beam BG4 in Fig. 9 had a longitudinal reinforcement ratio of 1.13% (3ϕ12 mm GFRP bars in the tension zone), a transverse reinforcement ratio of 0.65% (stirrup spacing of 200 mm), a 23.4 N/mm^2 cube strength and a 5.4 N/mm^2 modulus of rupture. The beam failed with 4 pure shear cracks, 4 flexural cracks within the loaded span and 7 flexural cracks at the shear span area of the beam. A maximum crack width of 1mm was measured with an average crack spacing of 71.88mm. The first crack appeared at 14 kN loading with a corresponding deflection of 7.99 mm. At 30 kN loading, the beam experienced a sudden brittle failure at a final deflection of 15.54 mm.

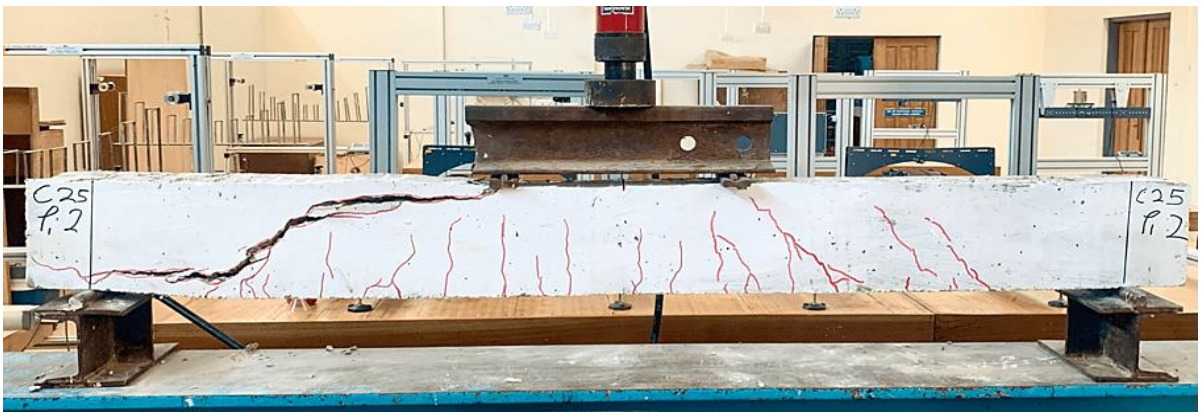

Fig. 10. Beam BG5 failure mode

The beam BG5 in Fig. 10 had longitudinal tensile reinforcement ratio of 1.13% (3ϕ12 mm GFRP bars in the tension zone), a transverse reinforcement ratio of 0.65% (stirrup spacing of 200 mm), a 23.4 N/mm^2 cube strength and a 5.4 N/mm^2 modulus of rupture. The beam failed with 5 pure shear cracks, 6 flexural cracks within the loaded span and 3 flexural cracks at the shear span area of the beam. A maximum crack width of 0.5 mm was measured with an average crack spacing of 68.9mm. The first crack appeared at 16 kN loading with a corresponding deflection of 5.19 mm. At 30 kN loading, the beam underwent a sudden brittle failure at a final deflection of 19.88 mm.

The beam BG6 in Fig. 11 had longitudinal tensile reinforcement ratio of 1.13% (3ϕ12 mm GFRP bars in the tension zone), a transverse reinforcement ratio of 0.65% (stirrup spacing of 200 mm), a 23.4 N/mm^2 cube strength and a 5.4 N/mm^2 modulus of rupture. The beam failed with 3 pure shear cracks, 6 flexural cracks within the loaded span and 5 flexural cracks at the shear span area of the beam. A maximum crack width of 0.5mm was measured with an average crack spacing of 91.57mm. The first crack occurred at 16 kN loading with a corresponding deflection of 4.66 mm. At 28 kN loading, the beam underwent a sudden brittle failure at a final deflection of 20.38 mm.

Beam BS1 shown in Fig. 12 is the control beam with traditional steel as reinforcement with same reinforcement configuration as the GFRP reinforced beams. The beam had longitudinal tensile reinforcement ratio of 0.7% (2ϕ12 mm steel bars in the tension zone), a transverse reinforcement ratio of 0.65% (stirrup spacing of 200 mm), a 23.4 N/mm^2 cube strength and a 5.4 N/mm^2 modulus of rupture. The beam failed with 6 pure shear cracks, 7 flexural cracks within the loaded span and 9 flexural cracks at the shear span area of the beam. A maximum crack width of 2mm was measured with an average crack spacing of 54.83mm. The first crack occurred at 20 kN loading with a corresponding deflection of 4.43 mm. At 30 kN loading, the beam underwent a failure at a final deflection of 11.39 mm.

Fig. 11. Beam BG6 failure mode

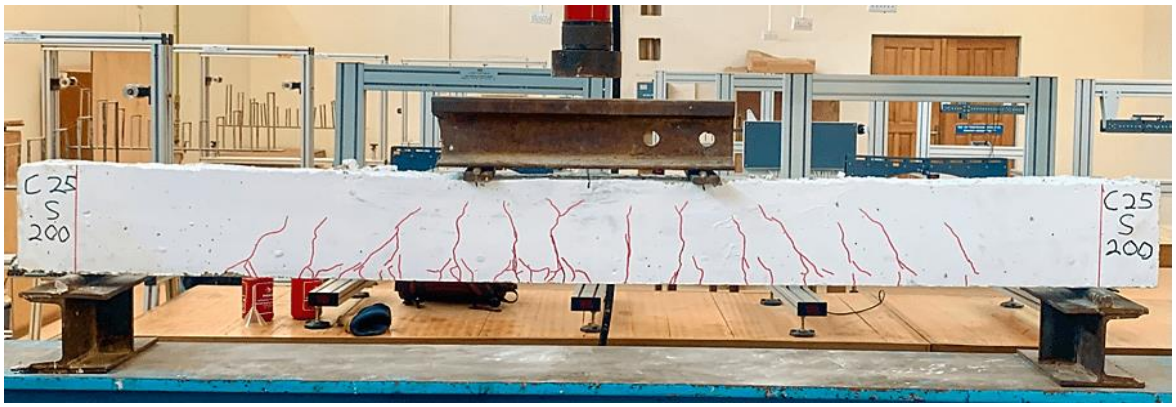

Fig. 12. Beam BS1 at failure

4.6 Effects of Concrete Strength on Deformation Characteristics of Beams Reinforced with GFRP Bars

Two strength grades of concrete were used in this experimental study, thus C25 and C30 which yielded compressive strength values of 23.4 N/mm^2 and 30.4N/mm^2 respectively. From Table 7, 23.4 N/mm^2 compressive strength of concrete achieved an estimated theoretical cracking load of 12.3 N/mm^2 compared to 14.4 N/mm^2 for 30.4N/mm^2, indicating a 17.1% increase in capacity of the GFRP RC beams. Similarly, beam BG1 of 23.4 N/mm^2 compressive strength recorded 28 kN experimental load compared to beam BG3 of 30.4 N/mm^2 compressive strength recorded higher values of 36 kN. A noticeable trend seen is that an increase in concrete strength from 23.4N/mm^2 to 30.4 N/mm^2 saw an increase in the load-carrying capacity by 28.6%. This finding is consistent with previous literature [4,19] that found that higher concrete strength contributed to efficient utilization of GFRP bar and increased load-carrying capacity.

4.7 Effects of Tensile Reinforcement Ratio on Strength and Deformation Characteristics of Beams Reinforced with GFRP Bars

From Table 7, beam BG1 with longitudinal tensile reinforcement ratio of 0.7% showed lower failure load compared to those with higher longitudinal tensile reinforcement ratio of 1.13% for GFRP bars. Similarly, GFRP reinforced beams with higher longitudinal ratio (BG4, BG5, BG6 = 1.13%) recorded lower final deflections of 19.88mm, 18.54mm and 20.38mm respectively, compared to final deflections of 28.86mm, obtained from lower tensile reinforcement ratio of beam (BG1, ρ=0.7%). This could be explained in light of the previous studies [9,24], which confirmed the enhanced stiffness of the beams with increased tensile reinforcement ratio.

5. CONCLUSIONS

This research investigated the structural behavior of concrete beams reinforced with GFRP bars as a promising alternative to conventional steel bars. The effects of variables of concrete compressive strength and tensile reinforcement ratios tested under a four-point monotonic loading system on the strength and deformational characteristics of GFRP-RC beams was examined. Based on the theoretical analysis and discussion of the experimental results, the following conclusions are drawn:

1. All GFRP reinforced concrete beams demonstrated typical bilinear elastic behavior until failure under static loading with evidence of reduced stiffness after cracking.
2. The GFRP-reinforced concrete beams experienced sudden concrete crushing due to shear-bond failure, diagonal tension failure, and flexural failure, in contrast to the steel-reinforced concrete beam, which failed due to yielding of the steel tension bars, as confirmed by the theoretical analysis.
3. For beam specimens reinforced with GFRP bars, an increase in concrete compressive strength from 23.4 N/mm^2 to 30.4 N/mm^2 resulted in a 28.6% increase in ultimate failure load.
4. Under identical load levels, higher concrete strength led to a greater number of cracks with reduced spacing and narrower crack widths compared to beams with lower concrete strength.
5. For beams with similar compressive strength and tensile reinforcement ratios, GFRP-reinforced beams were seen to exhibit higher deflections and greater number cracks in comparison to beams reinforced with steel.
6. Consistent with previous studies, increasing the longitudinal tensile reinforcement ratio of GFRP from 0.7% to 1.13% greatly increased the ultimate flexural capacity of beam specimens. Additionally, reduced deflections were noted.
7. Increasing the reinforcement ratio and concrete strength resulted in a larger number of cracks with narrower crack widths.
8. When compared to conventional steel-reinforced beams, GFRP reinforced concrete beams showed improved flexural performance and hence a remarkable structural behavior under bending loads, despite their brittle behavior. This is attributed to the relatively lower Young's modulus of elasticity, reduced ductility, and decreased stiffness obtained from the tensile test results and stress strain curve, when compared to traditional steel.

DISCLAIMER (ARTIFICIAL INTELLIGENCE)

Author(s) hereby declare that NO generative AI technologies such as Large Language Models (ChatGPT, COPILOT, etc) and text-to-image

generators have been used during writing or editing of manuscripts.

COMPETING INTERESTS

Authors have declared that no competing interests exist.

REFERENCES

1. MA E, Adam Abeer M, Habib Fatma A, El-Sayed, Taha A. Structural Behavior of High-Strength Concrete Slabs Reinforced with GFRP Bars. Polymers. 2021;13(17): 2997-NA.
   DOI: 10.3390/polym13172997.
2. Sheikh Zahra SAK. Replacement of steel with GFRP for sustainable reinforced concrete, Construction and Building Materials. 2018;160(NA):767–774.
   DOI: 10.1016/j.conbuildmat.2017.12.141
3. Maranan Allan GBM, Benmokrane Brahim, Karunasena Warna, Mendis Priyan. Evaluation of the flexural strength and serviceability of geopolymer concrete beams reinforced with glass-fibre-reinforced polymer (GFRP) bars, Engineering Structures. 2015;101(NA): 529–541.
   DOI: 10.1016/j.engstruct.2015.08.003
4. Tahmouresi Kasra BM, Mohseni Ehsan. Flexural response of FRP-strengthened lightweight RC beams: hybrid bond efficiency of L-shape ribbed bars and NSM technique, Archives of Civil and Mechanical Engineering. 2022;22(2).
   DOI: 10.1007/s43452-022-00410-y
5. Yang Doo Yeol J-MY, Shin Hyun Oh, Yoon Young Soo. Flexural strength and deflection evaluation for FRP bar reinforced HSC beams with different types of Reinforcing Bar and Fiber, Journal of the Korea Concrete Institute. 2011;23(4):413–420.
   DOI: 10.4334/jkci.2011.23.4.413.
6. Shaoce Chenggao DL, Xian Guijun. Environmental impacts of glass- and carbon-fiber-reinforced polymer bar-reinforced seawater and sea sand concrete beams Used in Marine Environments: An LCA Case Study, Polymers. 2021;13(1):154-NA.
   DOI: 10.3390/polym13010154.
7. Boateng GO, Kankam CK, Mansal EC, Afrifa RO, Kwarteng F, Ohene-Coffie F, Kpo SAK. Evaluating the Mechanical Properties of Fiberglass-Reinforced Polymer Bar. Journal of Engineering Research and Reports. 2024;26(7):150-60.
   Available:https://doi.org/10.9734/jerr/2024/v26i71200
8. Lu Hamdy JA M, Azimi, Hossein, Sennah, Khaled, Sayed-Ahmed, Mahmoud. Bond characteristics of glass-fibre-reinforced polymer bars in high-strength concrete, Proceedings of the Institution of Civil Engineers - Structures and Buildings. 2022;175(10):748–764.
   DOI: 10.1680/jstbu.19.00230.
9. Issa Ibrahim MSM, Elzeiny M, Sherif M. Influence of fibers on flexural behavior and ductility of concrete beams reinforced with GFRP rebars, Engineering Structures. 2011;33(5):1754–1763.
   DOI: 10.1016/j.engstruct.2011.02.014.
10. Taerwe L. Non-Metallic (FRP) Reinforcement for Concrete Structures: Proceedings of the Second International RILEM Symposium. CRC Press. 2004;18–24. [Online].
    Available:https://books.google.com.gh/books?id=dUVZDwAAQBAJ
11. Erfan Hossam AMH, Hatab E, Khalil M, El-Sayed, Taha A. The flexural behavior of nano concrete and high strength concrete using GFRP, Construction and Building Materials. 2020;247(NA):118664-NA.
    DOI: 10.1016/j.conbuildmat.2020.118664.
12. Sayan Sirimontree, Suraparb Keawsawasvong, Chanachai Thongchom. Flexural Behavior of Concrete Beam Reinforced with GFRP Bars Compared to Concrete Beam Reinforced with Conventional Steel Reinforcements, 淡江理工學刊. Dec. 2021;24(6).
    DOI: 10.6180/jase.202112_24(6).0009
13. Al-Sunna Kypros RP, Hajirasouliha Iman, Guadagnini Maurizio. Deflection behaviour of FRP reinforced concrete beams and slabs: An experimental investigation, Composites Part B: Engineering. 2012; 43(5):2125–2134.
    DOI: 10.1016/j.compositesb.2012.03.007
14. Toutanji Yong HD. Deflection and crack-width prediction of concrete beams reinforced with glass FRP rods, Construction and Building Materials. 2003; 17(1):69–74.
    DOI: 10.1016/s0950-0618(02)00094-6
15. Chang Yanlei YW, Wang Mifeng, Zhou Zhi, Ou Jinping. Bond durability and degradation mechanism of GFRP bars in seawater sea-sand concrete under the

coupling effect of seawater immersion and sustained load, Construction and Building Materials. 2021;307(NA):124878-NA.
DOI: 10.1016/j.conbuildmat.2021.124878.

16. Dong Gang ZW, Xu Yi-Qian. Experimental study on the bond durability between steel-FRP composite bars (SFCBs) and sea sand concrete in ocean environment, Construction and Building Materials. 2016;115(NA):277–284.
DOI: 10.1016/j.conbuildmat.2016.04.052
17. Jung J-SL, Bang Yeon, Lee, Kang-Seok. Experimental study on the structural performance degradation of corrosion-damaged reinforced concrete beams, Advances in Civil Engineering. 2019; 2019(NA):1–14.
DOI: 10.1155/2019/9562574
18. Mohammed SA, Said AI. A comparative study of the structural behavior of concrete beams Reinforced with Different Configurations of GFRP and Steel Bars, Jcoeng. Apr. 2024;30(04):200–218.
DOI: 10.31026/j.eng.2024.04.12
19. Adam MA, Said M, Mahmoud AA, Shanour AS. Analytical and experimental flexural behavior of concrete beams reinforced with glass fiber reinforced polymers bars, Construction and Building Materials. Jun. 2015;84:354–366.
DOI: 10.1016/j.conbuildmat.2015.03.057
20. Zhang Yu LZ, Shaowei Hu, Yang Jiasheng, Xia Lipeng. Identification of Bond-Slip Behavior of GFRP-ECC using smart aggregate Transducers, Frontiers in Materials. 2020;7(NA):165-NA.
DOI: 10.3389/fmats.2020.00165
21. Xie F, Tian W, Diez P, Zlotnik S, Gonzalez AG. Bonding performance of glass fiber-reinforced polymer bars under the influence of deformation characteristics, Polymers. Jun. 2023;15(12):2604.
DOI: 10.3390/polym15122604
22. Muhammad Faris MA R, Rafiq, Serwan. Investigation of flexural performance of concrete beams reinforced with glass fiber reinforced polymer rebars, The Journal of the University of Duhok. 2020;23(2):630–647.
DOI: 10.26682/csjuod.2020.23.2.49
23. Pilakoutas Maurizio KG, Neocleous Kyriacos, Matthys Stijn. Design guidelines for FRP reinforced concrete structures, Proceedings of the Institution of Civil Engineers - Structures and Buildings. 2011;164(4):255–263.
DOI: 10.1680/stbu.2011.164.4.255
24. Kim S-EK, Seung-Hun. Flexural behavior of concrete beams with steel bar and FRP reinforcement, Journal of Asian Architecture and Building Engineering. 2019;18(2):89–97.
DOI: 10.1080/13467581.2019.1596814
25. Ahmed Dilshad Kakasor HQJ, Yaseen, Sinan Abdulkhaleq. Flexural capacity and behaviour of geopolymer concrete beams reinforced with glass fibre-reinforced Polymer Bars, International Journal of Concrete Structures and Materials. 2020; 14(1):1–1.
DOI: 10.1186/s40069-019-0389-1.
26. British Standards Institution. BSI. 1377 Part 1 (1990): General Requirement and Sample Preparation. British Standard Institute, London; 1990.
27. ASTM. ASTM C150: Standard Specification for Portland Cement. Annual Book of ASTM Standards; 2001.
28. Indian standard, Recommended Guidelines for Concrete Mix Design, IS 10262:1982, Bureau of India Standard, New Delhi.
29. BS EN 12390-3 (2009). Testing hardened concrete-Part 3: Compressive Strength of Test Specimens. British Standard Institution, London; 2009.
30. ASTM D7205 (2006). Standard test method for tensile properties of fiber reinforced polymer matrix composite bars. ASTM Committee D30; 2006.

Peer-review history:
The peer review history for this paper can be accessed here:
https://www.sdiarticle5.com/review-history/122194